Journal of Thermal Analysis and Calorimetry, Vol. 73 (2003) 167–182

NON-ISOTHERMAL SHORT-RANGE-ORDER KINETICS OF BINARY ALLOYS AS INFLUENCED BY SOLUTE-VACANCY COMPLEXES
Alternative treatment

A. Varschavsky and E. Donoso[*]

Universidad de Chile, Facultad de Ciencias Físicas y Matemáticas, Instituto de Investigaciones y Ensayes de Materiales, IDIEM, Casilla 1420, Santiago, Chile

(Received January 13, 2002)

Abstract

A model describing the roles of bound and unbound vacancies is proposed in order to predict defect decay and short-range-order kinetics of quenched binary alloys during linear heating experiments. This is an alternative treatment of a previous approach. The model has been applied to the differential scanning calorimetry (DSC) curves of Cu–5 at.% Zn quenched from different temperatures. An expression to calculate the activation energy for migration of solute-vacancy complexes was also developed which make use of DSC trace data. A value of 89.12±0.32 kJ mol^{-1} was obtained for the above alloy. The relative contribution of bound and unbound vacancies to partition of effective activation energy corresponding to the ordering process as influenced by quenching temperature was also assessed.

Keywords: binary alloy, non-isothermal kinetics, solute-vacancy complexes

Introduction

The different features of short-range-order (SRO) in f.c.c. solid solutions have been profusely investigated for a long time by diffuse scattering of X-rays [1–6], by small-angle X-ray scattering [7], by electron microscopy and electron diffraction [8–12], by determination of elastic and plastic properties [13–15] and strengthening and fatigue properties [16–21], as well as by electrical resistivity [22–25] and thermal analysis [13, 14, 18, 26–31].

In contrast to usual experiments on SRO kinetics after quenching from rather high temperatures, some experiments are interested in the adjustment of the new equilibrium state of SRO established after small and sudden temperature changes [32–36] and others are now concerned with the influence of cold work [37–40]. However, quenching experiments still provides information about how excess vacancies frozen during the quench can affect the alloy ordering kinetics [41–45]. For instance,

* Author for correspondence: E-mail: edonoso@cec.uchile.cl

1388–6150/2003/ $ 20.00

Akadémiai Kiadó, Budapest
Kluwer Academic Publishers, Dordrecht

differential scanning calorimetry (DSC) of thermally disordered alloys reveals that two short-range-ordering processes generally take place in two stages, irrespective of the alloy system: stage-1 ordering at low temperatures is associated with the migration of excess vacancies, and stage-2 ordering at higher temperatures is due to the migration of equilibrium vacancies. The features displayed by the DSC traces have been explained quantitatively [43], predicting the relative importance of each stage and hence information was gained on the ordering process itself and vacancy behaviour.

Although one sees that while solid solution alloy systems, exhibiting SRO are being rather intensively investigated [46], there is very scarse description of the role of solute-vacancy complexes [47], which are determinant in explaining important features of several metallurgical processes [48–52]. There is then a need to examine the importance of such complexes in the ordering process, to the end of giving account of the observed behavior of the differential scanning calorimetry traces displayed after specific experiments, in which their presence can be evidenced.

An early work was published [53] in which the kinetics of non-isothermal short-range-order return was described by equations in which the effective activation energy of the overall process, together with the activation energy for bound vacancies was adjusted to a modified first order kinetic law. In the present paper, effective activation energies were calculated separately and hence the kinetic of the SRO reaction; computing previously the average activation energy for migration of bound vacancies by means of an expression considering the contribution of such complexes to the above process.

Chiefly, the present work *a*) designs experiments which characterize solute-vacancy complexes in a one stage ordering process, *b*) develop a model to assess activation energy for migration of these complexes from DSC data, *c*) discloses a model that predicts the return of unbound and bound vacancies to equilibrium, describing also the kinetics of reordering, *d*) tests its validity for Cu–5 at.% Zn, and *e*) performs a parametric study of the initial total defect concentration in order to establish its influence on the calculated DSC profiles.

Contribution of solute-vacancy complexes to a non-isothermal short-range-ordering (SRO) kinetic process

We are interested in this section in evaluating the relative concentration of solute-vacancy complexes after quenching to room temperature, where the same ordering condition as that at T_z (the actual freezing temperature) prevails, which in turn is the same existing at T_i, the inital temperature of the non-isothermal trace. After transients take place, were the unbound and bound vacancies redistribute at the peak onset temperature T_e, the total amount of defects still remains the same than those at T_z and hence at the inilial peak temperature T_i. Then, transient effects occur in the temperature interval $\Delta T=T_e-T_i$ (these temperatures are illustrated in Fig. 1). Also, it is the aim of the section to know the contribution of this defect type at T_p at which the reaction proceeds at its maximum rate. At T_f, the final trace temperature, equilibrium degree of order is reached and, as total vacancy concentration is negligible at this temperature compared with its value after quenching, it is then expected that solute-vacancy complexes are, too. Besides it is

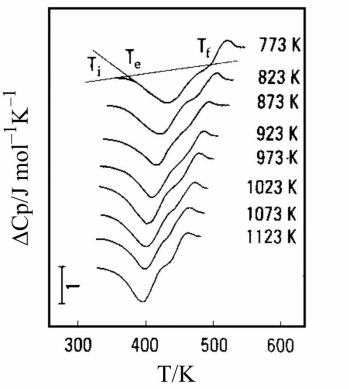

Fig. 1 DSC curves for Cu–5 at.% Zn quenched from the indicated temperatures. ϕ_r=0.33 K s^{-1}

worth pointing out that during quenching, vacancies can migrate because the cooling rate is finite in practical experiments. Above T_z, the reactions between the defects are considered to be in the thermal dynamical equilibrium because they are fast enough to maintain it between them during quenching from temperature T_q, as profusely reported [54–58]. Special interest is given to the determination of defect decay kinetics, as well as, to the effective non-isothermal short-range-ordering kinetics.

Initial defects concentration

In a one stage non-isothermal ordering process it was determined from the analysis of the DSC trace that the initial concentration of vacancies, as it was reported in a previous author's paper, [45] is given by

$$c_1(T_z)=\frac{2E\phi_r}{R\nu_{ot}T_p^2}\exp\left(\frac{E}{RT_p}\right) \tag{1}$$

where E is the experimental effective activation energy measured at peak temperature, ϕ_r is the heating rate, ν_{ot} is now the specific effective jump frequency when unbound and bound vacancies are present, that is when $c_t=c_u+c_b$, being c_u an c_b the unbound and bound vacancy concentration respectively, T_p is peak temperature and R the gas constant.

In Eq. (1), $c_t(T_z)$ represents the total concentration of defects at actual freezing temperature which participate in the thermal event. Also, as it will be infered latter on, $\nu_{ot}=\nu_{om}$, being ν_{om} the attempt frequency either for unbound or bound vacancies.

Now for moderate diluted alloys, as we will be concerned in the present work [59]:

$$\frac{c_b}{c_u}=\frac{Zx_t\exp\left(\frac{B}{RT}\right)}{1-(Z+1)x_t+Zx_t\exp\left(\frac{B}{RT}\right)} \tag{2}$$

where Z is the coordination number, x_t is the solute concentration and B is the solute-vacancy binding energy. Hereby:

$$\frac{c_b}{c_t}=\frac{Zx_t\exp\left(\frac{B}{RT}\right)}{1-(Z+1)x_t+2Zx_t\exp\left(\frac{B}{RT}\right)}=\Psi_b(T) \tag{3}$$

and

$$\frac{c_u}{c_t}=\frac{1-(Z+1)x_t+Zx_t\exp\left(\frac{B}{RT}\right)}{1-(Z+1)x_t+2Zx_t\exp\left(\frac{B}{RT}\right)}=1-\Psi_b(T) \tag{4}$$

As dynamical equilibrium exists during quenching, the concentrations $c_b(T_z)$ and $c_u(T_z)$ at the actual freezing temperature, can be readily calculated from:

$$c_b(T_z)=c_t(T_z)\Psi_b(T_z) \tag{5}$$

and

$$c_u(T_z)=c_t(T_z)(1-\Psi_b(T_z)) \tag{6}$$

A calculated freezing temperature $T_z^{'}$ can be estimated from [43]:

$$\frac{E_m}{RT_z}=\ln\left(\frac{RT_z^{'2}}{\phi_q\tau_0E_m}\right) \tag{7}$$

where $\tau_0=10^{-6}$ s [43] and ϕ_q is the cooling rate. It should be pointed out that the more mobile unbound vacancies with migration energy E_m determine T_z'. The actual freezing temperature $T_z=T_z'$ as long as $T_q>T_z'$, while if $T_q<T_z'$ then $T_z=T_q$, as will be illustrated latter in Fig. 2.

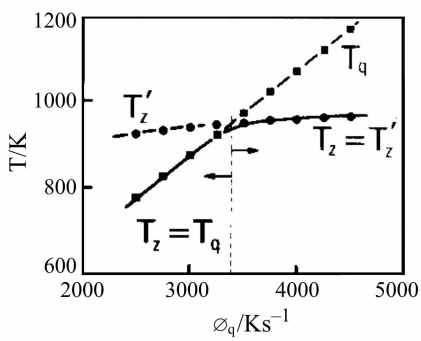

Fig. 2 Quenching (T_q) and calculated (T_z')freezing temperatures as a function of quench rate. The actual freezing temperature $T_z=T_z'$ for $T_q>T_z'$ while $T_z=T_q$ for $T_q<T_z'$

The effective migration activation energy

The effective migration activation energy measured during a DSC run by means of Kissinger method [60], is a weighted average value between those of unbound and bound vacancies, that is, $E=(1-\alpha)E_m+\alpha E_c$ where α is a strengthening factor, $E_c=E_m+\gamma B$, is the activation energy for migration of vacancy-solute complexes and γ is a material constant depending upon the solute. These expressions lead to:

$$E=E_m+\delta B \tag{8}$$

where $\delta=\alpha\gamma$. Although E can vary in the course of the reaction, we are here interested in its value at the reacted fraction corresponding to T_p. So α is presently representative of the contribution of bound to total vacancy concentrations at T_p. If theoretically all defect transport would occur by bound vacancies, which is not the case [61], $\alpha=1$, on the contrary for monovacancy transport only, $\alpha=0$. The value of α is constant along the DSC run when E is, too. Besides it is worth noticing that E_c is a mean quantity since it is well known that the mobility of solute-vacancy pairs depends on the frequency of vacancy jumps around the solute atom as well as on the frequency of solute-vacancy exchanges. There is not therefore a unique activation energy in general.

In order to assess α and γ we introduce previously the effective rate constant for the return of SRO to equilibrium. For a simultaneous unbound and bound vacancy mechanisms it can be stated as:

$$k_t = \nu_u c_u+\nu_b c_b \tag{9}$$

where ν_u and ν_b are the jump frequencies of unbound and bound vacancies. With the definition [61]:

$$\nu_t(c_u+c_b) = \nu_u c_u+\nu_b c_b \tag{10}$$

The idea contained in Eq. (3) is that the entire population of vacancies, unbound and bound, is assigned one effective jump frequency, ν_t, which is obtained as a weighted sum of simpler jump frequencies describing individual processes.

From Eqs (3), (4) and (10) one has:

$$\nu_t = \nu_u(1-\Psi_b(T))+\nu_b\Psi_b(T) \tag{11}$$

The jump frequencies are given by:

$$\nu_u=\nu_{om}\exp\left(-\frac{E_m}{RT}\right) \tag{12}$$

and

$$\nu_b=\nu_{om}\exp\left(-\frac{E_m+\gamma B}{RT}\right) \tag{13}$$

being E_m the migration activation energy for unbound vacancies. The attempt frequency ν_{om} is considered to be the same for unbound and bound vacancies [61]. Therefore the effective attempt frequency can be safely taken also as ν_{om} as stated before. Its value is given by ν_{om} =12 ν_0 exp ($\Delta S_m/R$) for f.c.c. alloys, where ν_0 is the Debye frequency and ΔS_m the activation entropy for free vacancies [45]. Thus:

$$\nu_t = \nu_{om} \exp\left(-\frac{E_m + \delta B}{RT} \right) \tag{14}$$

Substitution of Eqs (12), (13) and (14) in Eq. (11) yields:

$$\gamma = \frac{RT_p}{B} \ln\left(\frac{1}{1 + \frac{1}{\Psi_b(T_p)}\left[\exp\left(-\delta \frac{B}{RT_p} \right) - 1 \right]} \right) \tag{15}$$

Values for δ and T_p will be obtained from curves as shown latter on, hence an average value for γ can be readily calculated.

Effective defect decay kinetics

It is here considered that sink strengths of bound and unbound vacancies are equal, and that the total vacancy supersaturation follows a first like order kinetic path, as expected from its elimination at fixed sinks [62]. Also it is assumed that equilibrium at the end of the DSC trace at T_f is attained, at which the total vacancy concentration $c_t(T_f)$=0, since $c_t(T_z) >> c_t(T_f)$. Furthermore, the present analysis considers implicitly vacancy-solute complexes production and dissolution during the run since, as it will be justified latter on, a state of dynamical equilibrium prevails in the alloy during the heating process. It should be noticed that an explicit formulation for complexes production and dissociation is difficult to accomplish mathematically in no sufficiently diluted alloys, since it involves the solution of coupled differential equations containing no simple rate constants. This complex topic will be considered in a next paper, so the computed kinetic path here is a somewhat simplified one. Nevertheless, it gives enough insight of the main variations with temperature of all parameters involved during the heating DSC experiment. Therefore, using the effective vacancy jump frequency ν_t, defect supersaturation defined as $S=(c_t(T)-c_t^{eq})/(c_t(T_z)-c_t^{eq})$, decays according to:

$$\frac{dS}{dT} = -\frac{kS}{\phi_r} \tag{16}$$

being c_t^{eq} the total equilibrium defect concentration, ϕ_r the heating rate and $k=\nu_t \rho_t$, the rate constant, ρ_t is the effective sink density. For *a* one stage ordering process, as displayed under the present experimental conditions, the approximation c_t^{eq}=0 holds in principle. On the other hand, ρ_t is given by:

$$\rho_t = \rho_d + \rho_g \tag{17}$$

where ρ_d, the sink density for dislocations can be obtained from:

$$\rho_d = \frac{2\pi b^2 \delta}{\ln\left(\frac{r_s}{r_c}\right)} \tag{18}$$

in which r_s is the average distance between dislocations, r_c is the capture radius of a dislocation, δ is the dislocation density and b the atom jump distance. For grain boundaries, the sink density ρ_g is given by:

$$\rho_g = \frac{\lambda}{L^2} \tag{19}$$

where $\lambda = a_0^2/12$ for f.c.c. metals, a_0 is the lattice parameter and L the grain size. Using the definition of S given before and considering roughly as a first approximation that $c_t^{eq}=0$, integration of Eq. (16) yields:

$$c_t(T) = c(T_z)\exp\left[-\frac{(\rho_d+\rho_g)}{\phi_r}\int_0^T \nu_{om}\exp\left(-\frac{E}{RT}\right)dT\right] \tag{20}$$

or:

$$c_t(T) = c_t(T_z)\exp[-(\rho_d+\rho_g)\nu_{om}\theta(E,T)] \tag{21}$$

where θ, the reduced time is given by [63–65]:

$$\theta(E,T) = \frac{RT^2}{\phi_r E}\exp\left(-\frac{E}{RT}\right) \tag{22}$$

It is immediately evident from Eq. (21) that the total defect concentration does not obey a simple Arrhenius equation even though the decay curve, which must be solved numerically is purely exponential.

It should be stressed that during the DSC run, as considered before, $c_t(T)$, $c_u(T)$ and $c_b(T)$ are in dynamical equilibrium between them at states characteristic of temperatures higher than T, the temperature at which the alloy is. These states vary steadily from their initial values at T_z. Such consideration stems from the fact that if during quenching dynamical equilibrium between defects is attained [57], the more so when heating during the DSC run because the heating rate is orders of magnitude lower than the quench rate. Therefore defect decay rates should permanently adjust through the transfer function $\Psi_b(T)$ to maintain equilibrium between c_u, c_b and c_t. Furthermore, it has been demonstrated [47] that the formation of vacancy–solute pairs occurs on the quick time scale for vacancy relaxations, and for most purposes the numbers of vacancy–solute pairs can be assumed to be in equilibrium with the state of chemical order in the alloy. Henceforth, the decay kinetics of total amount of vacancies follows the relationship:

$$c_b(T) = \Psi_b(T)c_t(T) \tag{23}$$

and

$$c_u(T) = [1-\Psi_b(T)]c_t(T) \tag{24}$$

It should be kept in mind that these equations and also Eq. (21) give approximate determinations, since in its derivation the composite quantity ν_t is involved, which is an effective jump frequency. Decay defect curves will be shown latter on in section concerning numerical results.

Effective non-isothermal short-range-ordering kinetics

As long as the ordering process can be described by a first-order kinetic law, as can be done for most binary alloy system [66], the differential equation for the transformed fraction y, under a linear rate becomes:

$$\frac{dy}{dT}=\frac{k_t}{\phi_r}(1-y) \tag{25}$$

where $k_t=\nu_t c_t$ is the rate constant. Integration yields:

$$y=1-\exp\left[-\frac{1}{\phi_r}\int_0^T \nu_t c_t dT\right] \tag{26}$$

Since:

$$\nu_t c_t = \nu_u c_t(1-\Psi_b(T))+\nu_b c_t \Psi_b(T) \tag{27}$$

hence Eq. (25) becomes:

$$y = 1-I_u I_b \tag{28}$$

where

$$I_u=\exp\left[-\frac{1}{\phi_r}\int_0^T \nu_u c_t (1-\Psi_b(T))dT\right] \tag{29}$$

and

$$I_b=\exp\left[-\frac{1}{\phi_r}\int_0^T \nu_b c_t \Psi_b(T)dT\right] \tag{30}$$

The mathematics of Eq. (28) is not transparent and it must be solved numerically.

In the following, we will apply these simplified analyses here developed to evaluate by means of DSC the defect and ordering kinetics in a high rate quenched copper-zinc solid solution from different temperatures, in which equilibrium SRO is reached in one stage during a DSC experiment.

Numerical application concerning Cu–5 at % Zn

The alloy studied contained, 5.1 mass% zinc (99.97 mass%). It was prepared in a Baltzer VSG 10 vacuum induction furnace from electrolytic copper (99.95 mass%) in a graphite crucible. The ingot was subsequently forged at 923 K to a thickness of 10 mm, pickled with a solution of nitric acid (15% in distilled water) to remove surface oxide, annealed in a vacuum furnace at 1123 K for 36 h to achieve complete homogeneity, and cooled in the furnace to room temperature. It was then cold-rolled to 1.5 mm thickness with intermediate annealing periods at 923 K for one hour. After the last anneal, the material was finally rolled to 0.75 mm thickness (50% reduction).

Subsequent heat treatments were performed at different temperatures for one h, followed by quenching in a high rate quenching device developed in our laboratory. The quench time was measured with an oscilloscope and estimated in 200 ms. Such high quench rates were used in order to promote a one stage ordering process via an excess of free and bound vacancies from all selected quenching temperatures. That is, by minimizing defect losses during the quench, sufficient defects in excess are available to reach and equilibrium state of short-range-order. Otherwise, reordering involves two-stage processes, the first assisted by excess defects and the second by equilibrium defects [41, 42]. A one stage process facilitates the separation of the rolles of unbound and bound vacancies.

Microcalorimetric analysis of the samples was performed in a DuPont 2000 thermal analyser. Specimen discs of 0.75 mm thickness and 6 mm diameter were prepared. Differential scanning calorimetric measurements of the heat flow were made by operating the calorimeter in the constant heating mode (heating rates of 0.83, 0.33, 0.17, 0.083 and 0.033 K s^{-1}). Runs were made from room temperature to 740 K. To increase the sensitivity of the measurements, a high purity, well-annealed copper disc, in which no thermal events occur over the range of temperatures scanned, was used as a reference. In order to minimize oxidation, dried argon ($0.8 \cdot 10^{-4}$ m^3 min^{-1}) was passed through the calorimeter.

DSC curves and the role of solute-vacancy complexes in the ordering process

Typical DSC curves for the alloy under study at the indicated quenching temperatures are shown in the differential heat capacity ΔC_p *vs*. temperature (T) curves at a heating rate ϕ_r=0.33 K s^{-1} in Fig. 1. They are characterized by one exothermic peak, namely stage 1 and one endothermic peak, stage 2. Stage 1 has been reported in the literature in connection with short-range order development assisted by excess defects, while stage 2 has been associated with a disordering process [44, 45]. It can be observed that in the present type of experiments (high quench rates), all stages shift to higher temperatures as the quenching temperature decreases. Stage 1 and 2 shifting, will be associated with the relative increasing importance of solute-vacancy complexes as quenching temperature is lowered. The enthalpimetric features of these curves will be considered in a next work, as they are not be involved within the scope of the models here developed.

In order to support the evidence that solute-vacancy complexes play an important role in the reordering process, the characteristic parameters of these curves,

namely overall apparent activation energy (E), peak temperature (T_p) and the factor $\delta=(E-E_m)/B$ according to Eq. (8), were determined for the different quenching temperatures (T_q) employed. Activation energies were calculated at reacted fractions corresponding to T_p according to Kissinger method [60]. The corresponding curves are not included for brevity sake. It should be noticed that, although based in a different mathematical formalism, effective energy values resulted similar to those adjusted with the previous treatment [53]. This might stem from the fact that the pre-exponential factor of the Arrhenius constant k_0, approaches the mean value of $c_t(T)\nu_{ot}$ in the temperature interval (T_e, T_f). All above data are summarized in Table 1.

With the values of E, T_p and the heating rate ϕ_r, the total defect concentration $c_t(T_z)$ at actual freezing temperature after quenching can be determined from Eq. (1) taking $\nu_{ot}=\nu_{om}=4.3\cdot10^{14}$ s^{-1} [44]. As can be seen, this computation is made on the basis of the experimental reordering DSC traces. The contribution of bound and unbound vacancy concentrations at peak initiation (T_i) can be readily calculated by means of Eqs (5) and (6), previous computation of the equilibrium transfer function $\Psi_b(T_z)$ at actual freezing temperature. The calculated freezing temperature T_z' is determined from Eq. (7). Cooling rates were calculated as $\phi_q=(T_q-T_o)/t_q$, where the quench temperature is T_0=273 K. A quench time t_q=200 ms was estimated as stated earlier. Also as mentioned before, when $T_q<T_z'$ for determined quenching conditions T_q prevails, that is the actual freezing temperature $T_z=T_q$ and all defects in equilibrium at T_q are quenched-in. On the contrary if $T_q>T_z'$, $T_z=T_z'$, that is, the actual freezing temperature is equal to the calculated one. This conditions are illustrated in Fig. 2. The quenched-in defect concentrations $c_t(T_z)$, $c_u(T_z)$ and $c_b(T_z)$ as a function of the quenching temperature are shown in Fig. 3. They will be used as boundary values in defect and SRO kinetic evaluations. As expected, quenched-in defects, bound or unbound, increase with quenching temperature.

Table 1 Quench and peak temperatures, effective activation energies and factor δ at T_p for Cu–5 at.% Zn

T_q/K	T_p/K	E/kJ mol^{-1}	δ
773	433	85.0±0.7	0.28
823	425	84.7±0.7	0.26
873	419	84.3±0.7	0.24
923	414	83.9±0.6	0.21
973	409	83.5±0.6	0.19
1023	405	83.1±0.6	0.16
1073	401	82.5±0.6	0.12
1123	398	81.8±0.6	0.09

In Fig. 4, the ratio $(c_b/c_u)_{T_z}$ *vs.* T_q is plotted. The main result obtained in this plot lies in the fact that such ratio increases with decreasing quenching temperature, that is, bound vacancies becomes more important relative to unbound ones, in good correlation with the increasing values of overall activation energy with decreasing T_q val-

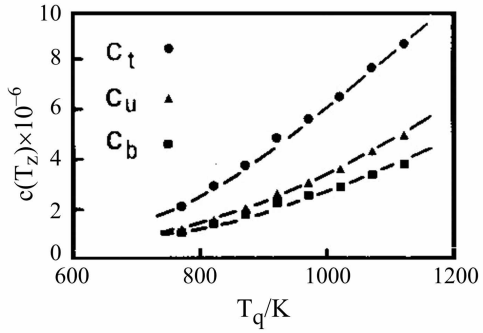

Fig. 3 Bound (c_b), unbound (c_u) and total vacancy concentration at freezing temperature as a function of the quenching temperature

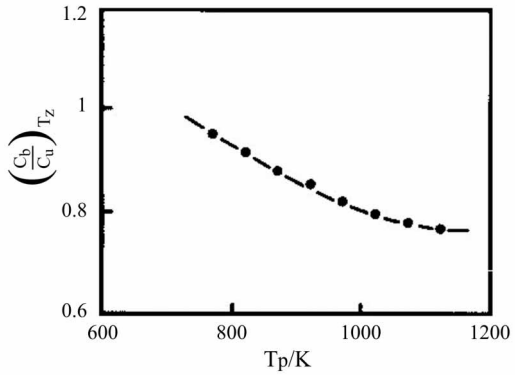

Fig. 4 Ratio of bound to unbound vacancy concentration at freezing temperature as a funcion of quenching temperature

ues. Such correlation migth be indicative that the observed increase in overall activation energy is attributable to the presence of a larger amount of less mobile bound vacancies during the ordering process. As stated before, both defect types are in equilibrium between them during the whole DSC run.

Such findings deserve to assess the activation energy for migration of bound vacancies, $E_c=E_m+\gamma B$. The factor γ was calculated from Eq. (15). Values for δ at T_p are taken from Table 1. After computations, an average value $\gamma=0.57\pm0.02$ was obtained. Activation energy for unbound vacancies was obtained by extrapolation of values previously calculated in [44]. An improved value of B=16.0 kJ mol^{-1} was computed after accurate iteration of Eq. (6) of [44]. Hence, for bound vacancies:

$$E_c= 89.12\pm0.32 \text{ kJ mol}^{-1}$$

thus confirming the lower mobility of bounded vacancies as compared with:

$$E_m= 80 \text{ kJ mol}^{-1}$$

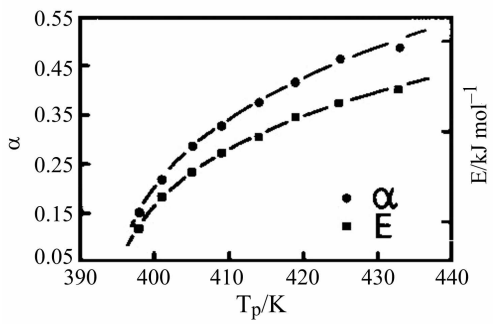

Fig. 5 Parameter α and effective activation energy (E) as a function of DSC trace peak temperature (T_p)

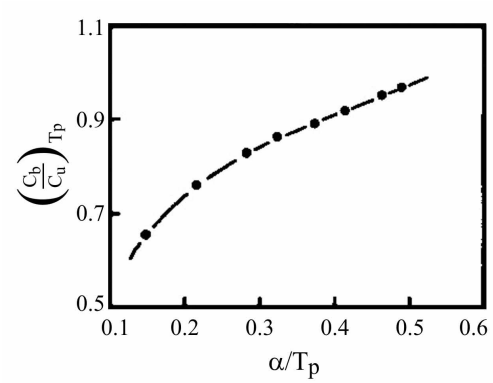

Fig. 6 Ratio of bound to unbound vacancies as a function of parameter α at peak temperature (T_p)

for unbound vacancies. Knowledge of γ, which is quite insensitive to temperature variations round $T_{p,}$ allows to determine readily the strengthening factor for bounded vacancies, α.

A plot of α and E *vs*. T_p, at which ordering is taking place as its maximum rate, is in perfect agreement with previous results as shown in Fig. 5. Evenmore, a linear dependence between $(c_b/c_u)_{T_p}$ and α is observed in Fig. 6 for low quenching temperatures. Such dependence breaks down as this ratio decreases when T_q becomes higher. The range covered by $(c_b/c_u)_{T_p}$ in the linear part of the plot is lower than the one covered by α, leading to the conclusion that α is very sensitive to small variations of this ratio for the lower quenching temperatures. All above findings demonstrate unequivocally that bound vacancies play an important role in the features displayed by the curves, basically in the increase of E with decreasing T_q values.

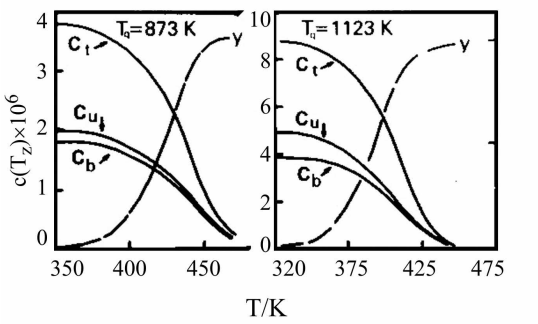

Fig. 7 Bound, unbound and total vacancy concentration decay curves during a DSC run at ϕ_r=0.33 K s^{-1} after quenching from the indicated temperatures. The experimental SRO reacted fractions are also shown

Defect annihilation and orderig kinetics

Before computing defect decay curves according to Eqs (21–24), dislocation sink density for dislocations and grain boundaries must be estimated. For a typical annealed material the dislocation density is $\delta=10^7$ cm^{-2} [43]. For this value the term $2\pi b^2/\ln(r_s/r_c)$ of Eq. (18), which is relatively insensitive to the dislocation density for annealed alloys was $4.4\cdot10^{-16}$ cm^2 and hence $\rho_d=4.4\cdot10^{-9}$. The measured grain size was L=100 μm, a_0=0.36 nm and $\lambda=1.1\cdot10^{-16}$ cm^2, thus from Eq. (19) $\rho_g=1.1\cdot10^{-12}$, which is negligible compared with ρ_d for the above grain size. Initial boundary values for $c_t(T_z)$, $c_b(T_z)$ and $c_u(T_z)$ were obtained for the chosen quenching temperatures from Fig. 3 and E values were taken for such temperatures from Table 1. Decay defect curves for T_q=873 K and T_q=1123 K are shown in Fig. 7 at a heating rate of 0.33 K s^{-1}. Superimposed to these curves are the experimental reacted fractions obtained from the corresponding curves as $y=a_t/A$, where a_t is the area under the peak to temperature T and A is the total area of the peak. For reaching correspondence between decay and y curves the range T_e–T_f, the adjusting parameter taken was E_m. The best fit in this

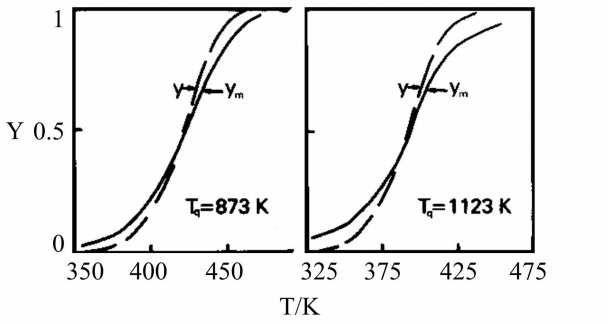

Fig. 8 Experimental (y) and model based (y_m) SRO reacted fractions during a DSC run at ϕ_r =0.33 K s^{-1} in samples quenched from the indicated temperatures

range was achieved with $E_m \approx 77.5$ kJ mol^{-1} for both quench temperatures, which is very satisfactory on evaluation of the defect decay model here developed.

In Fig. 8 the experimental and theoretical reacted fractions for reordering are compared for the same quenching temperatures and heating rate as employed in Fig. 7. The best fit was obtained in both cases for E_m=76 kJ mol^{-1} which is still fairly good if compared with previous determined value E_m=80 kJ mol^{-1}.

Conclusions

The present study leads to the conclusion that the relative importance of solute-vacancy complexes can be quantified by a simple model which predict defect decay and ordering kinetics of quenched alloys during non-isothermal conditions. Comparison of the model based kinetic paths with the experimental ones shows fair good consistency in Cu–5 at.% Zn. Also an expression to calculate the activation energy for migration of bound vacancies was determined making use of DSC data, giving a quite reasonable value for above alloy. The contribution of bound and unbound vacancies to the partition of effective activation energy was also assessed. The relative contribution of bound vacancies becomes more important as quenching temperature decreases.

* * *

The authors would like to acknowledge the Fondo de Desarrollo Científico y Tecnológico (FONDECYT) for financial support, Project 1020127, and the Facultad de Ciencias Físicas y Matemáticas, Universidad de Chile, for facilities provided for this research.

References

1 B. Borie and C. J. Sparks Jr., Acta Crystallogr., 17 (1964) 827.
2 V. I. Iveronova, A. A. Katnslelson and G. P. Revkevich, Fiz. Met. Metalloved., 26 (1968) 106.
3 R. O. Scattergood, S. C. Moss and M. B. Bever, Acta Metall., 18 (1970) 1087.
4 N. Kuwano, Y. Tomokiyo, C. Kinoshita and T. Eguchi, Trans. Jpn. Inst. Met., 15 (1974) 338.
5 Y. Kitano and Y. Kimura, J. Phys. Soc. Jpn., 32 (1972) 1430.
6 J. E. Epperson, P. Furnrohr and C. Ortiz, Acta Crystallogr., A34 (1978) 667.
7 R. W. Cahn and R. G. Davies, Philos. Mag., 5 (1960) 1119.
8 W. Gaudig and H.Warlimong, Z. Metallkd., 60 (1969) 488.
9 Y. Tomokiyo, N. Kuwano and T. Eguchi, J. Phys. Soc. Jpn., 35 (1973) 618.
10 Y. Tomokiyo, K. Kabu and T. Eguchi, Jpn. Inst. Met., 15 (1974) 39.
11 A. Varschavsky, M. I. Pérez and T. Löbel, Metall. Trans., 6A (1975) 577.
12 W. Gaudig and H. Warlimont, Acta Metall., 26 (1978) 709.
13 J. M. Popplewell and J. Crane, Metall. Trans., 2 (1971) 341.
14 C. Kinoshita, T. Tomokiyo, H. Matsuda and T. Eguchi, Trans. Jpn. Inst. Met., 14 (1973) 91.
15 M. Zchetbauer, L. Trieb and H. P. Aubauer, Z. Metallkd., 26 (1976) 431.
16 A. Varschavsky, Mater. Sci. Eng., 22 (1976) 141.
17 A. Varschavsky and E. Donoso, Mater. Sci. Eng., 32 (1978) 65.
18 E. Donoso and A. Varschavsky, Mater. Sci. Eng., 37 (1979) 151.

19 A. Varschavsky and E. Donoso, Mater. Sci. Eng., 40 (1979) 119.
20 A. Varschavsky and E. Donoso, Mater. Sci. Eng. A, 10 (1988) 231.
21 A. Varschavsky and E. Donoso, Mater. Sci. Eng. A, 104 (1988) 141.
22 G. Veith, L. Trieb, W. Puschl and H. P. Aubauer, Phys. Stat. Sol., 27 (1975) 59; Scr. Metall., 9 (1975) 737.
23 A. Varschavsky and E. Donoso, Thermochim. Acta, 69 (1983) 341.
24 M. J. S. Wechsler and R. H. Kernohan, Acta Metall., 7 (1959) 599.
25 L. Trieb and G. Veith, Acta Metall., 26 (1978) 185.
26 C. R. Brooks and E. E. Stansbury, Acta Metall., 11 (1963) 1303.
27 Y. Tomokiyo, N. Kuwano and T. Eguchi, Trans. Jpn. Inst. Met., 26 (1975) 489.
28 A. Varschavsky, Metall. Trans., 13A (1982) 801.
29 A. Varschavsky and E. Donoso, Metall. Trans., 14A (1983) 875.
30 A. Varschavsky and E. Donoso, Metall. Trans., 15A (1984) 1999.
31 A. Varschavsky and E. Donoso, J. Mater. Sci., 21 (1986) 3873.
32 W. Pfeiler, P. Meisterle and M. Zehetbauer, Acta Metall., 32 (1984) 1053.
33 W. Pfeiler, R. Reihsner and D. Trattner, Scr. Metall., 19 (1985) 199.
34 M. Migschitz, F. Laugmayr and W. Pfeiler, Mater. Sci. Eng. A, 177 (1994) 217.
35 M. Migschitz, W. Garlipp and W. Pfeiler, Mater. Sci. Eng. A, 214 (1996) 17.
36 T. Doppler and W. Pfeiler, Phys. Stat. Sol.(a), 131 (1992) 131.
37 M. Spanl, P. Rosenkranz and W. Pfeiler, Mater. Sci. Eng. A, 234 (1997) 541.
38 M. Migschitz, A. Korner, W. Garlipp and W. Pfeiler, Acta Metall. Mater., 44 (1996) 1359.
39 W. Garlipp, M. Migschitz and W. Pfeiler, In: Solid–solid phase transformations, Ed. by W. C. Johnson, J. M. Howe, D. E. Laughlin and W. A. Soffa, The Minerals, Metals and Materials Society 1994, p. 461.
40 M. Migschitz and W. Pfeiler, Mater. Sci. Eng. A, 206 (1996) 155.
41 A. Varschavsky and E. Donoso, Mater. Sci. Eng.A, 145 (1991) 95.
42 A. Varschavsky, Thermochim. Acta, 203 (1992) 391.
43 A. Varschavsky and M. Pilleux, Mater. Letts., 17 (1993) 364.
44 E. Donoso and A. Varachavsky, J. Thermal. Anal., 45 (1995) 1419.
45 A. Varschavsky and E. Donoso, Mater. Sci. Eng. A, 212 (1996) 265.
46 J. Plessing, Ch. Achmus, H. Neuhäuser, B. Schönfeld and G. Kostorz, Z. Metallkd., 88 (1997) 630.
47 B. Fultz In: Kinetics of ordering transformations in metals, Ed. by J. Chen and V. K. Vasudevan. The minerals, metals and materials society 1992, p. 121.
48 C. R. S. Beatrice, W. Garlipp, M. Cilense and A. T. Adorno, Scr. Metall. Materiallia, 32 (1995) 23.
49 L. S. Chang, E. Rabkin, B. Baretsky and W. Gust, Scr. Materiallia, 38 (1998) 1033.
50 T. Kasuya and M. Fuji, J. Application Phys., 83 (1998) 3039.
51 J. Baker, C. J. Girard and C. A. Sholl, Philos. Mag. A, 74 (1996) 543.
52 J. Wolf, M. Franz, J. E. Kluin and D. Schmid, Acta Materiallia, 45 (1997) 4759.
53 A.Varschavsky and E. Donoso, J. Therm. Anal. Cal., 63 (2001) 397.
54 A. C. Dasmak and G. J. Dienes, Phys. Rev., 120 (1960) 99.
55 F. Cattaneo and E. Germagnoli, Phys. Rev., 124 (1961) 414.
56 M. Doyama, Phys. Rev., 148 (1966) 683.
57 N. K. Srinivasan and V. Ramachandran, Phys. Stat. Sol., 36 (1969) 673.
58 M. Doyama, Mater. Chem. Phys., 50 (1997) 106.

59 D. V. Ragone, Thermodynamics of Materials, Vol. 2., Wiley 1995, p. 73.
60 H. E. Kissinger, Anal. Chem., 28 (1957) 1702.
61 L. K. Mansur, Acta Metall., 29 (1981) 375.
62 M. Halbwachs and J. Hillairet, Phys. Rev., B18 (1978) 4927.
63 C. Sandu and R. Singh, Thermochim. Acta, 159 (1990) 267.
64 E. J. Mittemeijer, J. Mater. Sci., 27 (1992) 3977.
65 A. Borrego and G. Gonzalez-Docel, Mater. Sci. Eng. A., 245 (1998) 10.
66 W. Pfeiler, Acta Metall., 36 (1988) 2.